Improved estimation of the temporal decay function of *in vivo* metabolite signals

D. van Ormondt, R. de Beer
Applied Physics
TU Delft, NL

J.W.C. van der Veen
MRS Core Facility
NIMH, NIH
Bethesda, USA

D.M. Sima
ESAT-SCD
KU Leuven, BE

D. Graveron-Demilly
CREATIS-LRMN, Univ Lyon 1
Villeurbanne, FR

***Abstract*—MRI-scanners enable non-invasive, *in vivo* quantitation of metabolites in, *e.g.*, the brain of a patient. Among other things, this requires adequate estimation of the unknown temporal decay function of the complex-valued signal emanating from the metabolites. We propose a method to render a current decay estimator more simple, accurate, and robust, and test it on a simulated signal comprising contributions from ten metabolite species and scanner noise.**

***Index Terms* — metabolite quantitation, signal-decay function, semi-parametric estimation, low-pass filter.**

I. Introduction

Magnetic Resonance Imaging, MRI, is the only technique that enables non-invasive, *in vivo* quantitation[1] of metabolites in, *e.g.*, the brain of a patient. To be more precise, MR Spectroscopy, MRS, a modality of MRI, is the correct name of this technique.

The present paper is a follow-up of our paper in Proceedings ICTOPEN 2013 [1], entitled "Error-Bars in Semi-Parametric[2] Estimation". In that study, we pointed out that the model function of the temporal decay of an *in vivo* MRS signal is usually unknown due to natural tissue inhomogeneity in a patient. Although the form of the decay has only nuisance value in the clinic, ignorance about this form unavoidably causes bias in the estimated metabolite concentrations, much to the detriment of medical practice.

In the previous paper we approximated the unknown true decay by a surrogate, *analytical* physical model function, namely mono-exponential decay [1]. The decay constant was estimated from the data. This procedure, although used in many MRS applications, can give rise to considerable, yet undetectable, bias.

In the present paper, on the other hand, we estimate the decay function *numerically* – *i.e.*, in contrast to using an analytical form – and substitute the result into the model of the MRS signal. Unlike previous methods for numerically estimating the decay, see *e.g.* [2],[3],[4] and references therein, the estimate is not easily perturbed by measurement noise in the MRS signal. Details of the new method are still under investigation.

The estimated decay is in turn used to complete the model function of the MRS signal. Finally, the model parameters of medical interest can be estimated by non-linear least-squares (NLLS) fitting of the MRS model function to the *in vivo* measured MRS signal [4].

[1] An alternative term for quantitation is quantification.

[2] Semi-parametric means that the model function used for describing/analysing a physical phenomenon is only partly known.

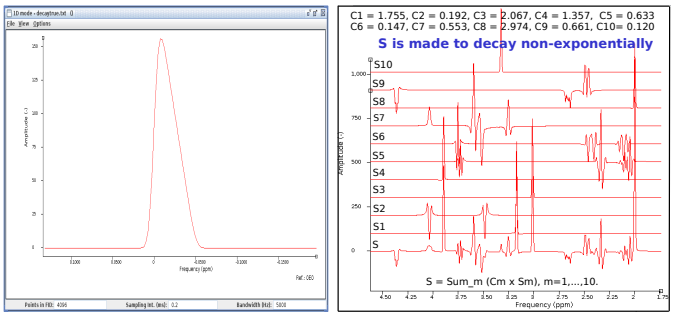

Figure 1. **Left:** Re[FFT($d(t)$)], where $d(t)$ is here the version used in the simulation of the MRS signal $s(t)$. Recall that the spectroscopic lineshape, in the frequency domain, is the Fourier Transform of the temporal decay $d(t)$ of $s(t)$. **Right:** Re[FFT($s(t)$)] (noiseless) and Re[FFT($s_m(t)$)]; from [1]. In MRS, the frequency is expressed in units of ppm, while the spectrum is displayed in reversed order, *i.e.*, running from high to low values. The numbers along the axes can be zoomed to improve reading. Graphs made with 'jMRUI' [5].

Sec. II is devoted to the new method for numerically estimating the decay function. Sec. III treats subsequent NLLS fitting of the MRS model function to a simulated *in vivo* MRS signal with thousand different added noise realisations (Monte Carlo procedure). Sec. IV discusses various aspects of the new method and the Monte Carlo results. Finally, Sec. V sums up conclusions.

II. Methods

A. *Model function [1]*

An *in vivo* MRS signal, $s(t)$, is complex-valued and is acquired in the time-domain. Apart from noise, we model it here by

$$s(t) = d(t)\, e^{\imath\varphi_0} \sum_{m=1}^{M} c_m\, s_m(t)\, e^{\imath\,(2\pi\triangle\nu_m t+\varphi_m)} \quad (1)$$

$$= d(t)\, e^{\imath\varphi_0}\, s(t)^{\text{no\_decay}} \quad (2)$$

in which t is time, $\imath^2 = -1$, φ_0 is an overall phase, $\triangle\nu_m$ and φ_m are nuisance parameters (for clinicians), and $m = 1, \ldots, M$ are the indices of the metabolites.

Furthermore, c_m, $m = 1, \ldots, M$ are the amounts or concentrations of the metabolites, to be estimated. They are the most important pieces of information for clinicians. The $s_m(t)$, $m = 1, \ldots, M$ are known, non-decaying theoretically computed versions of the model functions of the metabolites. The definition of $s(t)^{\text{no\_decay}}$ follows from comparing Eqs. (1) and (2).

$d(t)$ governs the decay of the signal[3] As mentioneed in the Introduction, the form of $d(t)$ is *a priori* unknown due to tissue heterogeneity in humans or animals. We devised a new method for numerically estimating it from the data. Our previous methods are sensitive to noise in the data. Below we show how the effect of noise can be alleviated.

From Eq. (2), one has

$$d(t) \approx \frac{s(t)\, e^{-\imath\varphi_0}}{s(t)^{\text{no\_decay}}} = \frac{|s(t)|}{|s(t)^{\text{no\_decay}}|}\, e^{\imath\phi(t)} \qquad (3)$$

where the approximation sign '$\approx$' indicates that this relation is satisfied only when all physical parameters contained in the denominator, $s(t)^{\text{no\_decay}}$, have the true value and measurement noise is absent from the numerator; $\exp(\imath\phi(t))$ is a complex-valued phase factor.

In practice, neither of the two conditions mentioned above is satisfied. As for the 1st condition, reasonable starting values of the physical parameters can be obtained by initially fitting Eq. (1) to the data $s(t)$ using the simple analytical decay function $d(t) = \exp(\alpha t)$, where $\alpha < 0$. As for the 2nd condition, at values of t where the size of the oscillatory signal $s(t)$ happens to be about equal to, or smaller than, that of the noise, the value of the division $|s(t)|/|s(t)^{\text{no\_decay}}|$ in Eq. (3) can be severely perturbed, resulting in a spiky appearance of $d(t)$. It is this latter phenomenon that was successfully addressed in the present work. The next Subsection is devoted to our method.

B. *Reduction of the sensitivity of Eq.(3) to noise*

In the past, the spiky appearance mentioned above was addressed mainly *after* executing the division, *i.e.*, after the damage was done. Here, we intervene before executing the division, and this in such a way that it is rendered harmless. To be able to do so, one must identify the main cause of the sensitivity to noise. As already indicated in the previous Subsection, the heart of the problem lies in the *oscillatory* nature of MRS signals. Therefore, we propose to remove the oscillations prior to division, and this using a conventional, 'Butterworth 3', low-pass filter [6]. For optimal performance, it is important to avoid edge effects of the filter at $t = 0$, the starting point of the signal at its maximum strength. To this end, we symmetrise the signal by reflection with respect to $t = 0$, thereby doubling its duration. Subsequently, we

[3] If the MRI/MRS scanner operates at a magnetic field of $\geq$ 11.7 Tesla, the decays of all metabolite species may be equal due to micro-susceptibility effects [1]. See Re[FFT($d(t)$)] used in this work in Fig. 1.

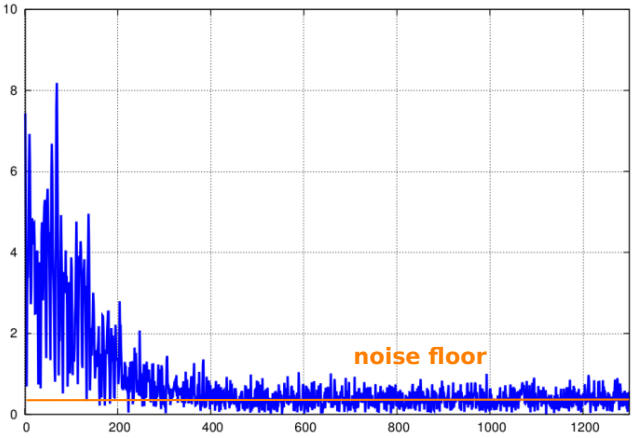

Figure 2. Absolute value of the complex-valued MRS signal, $|s(t)|$, in the numerator of the fraction in Eq. (3). Apparently, the signal has decayed into the noise by sample point 500. As many as 10 metabolites contribute to the signal [1]; see right-hand side of Fig. 1.

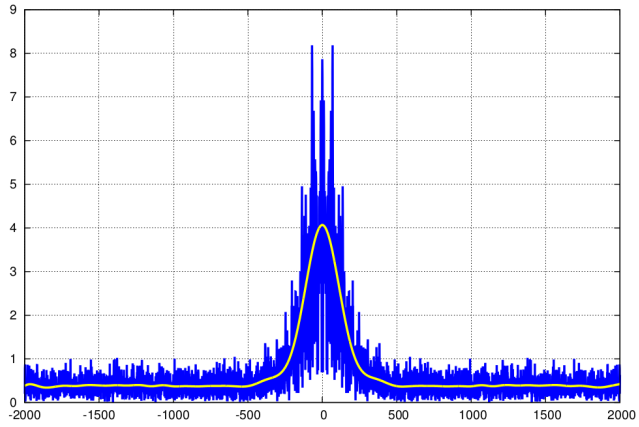

Figure 3. Blue: Same as Fig. 2, but now symmetrised by including reflection w.r.t. $t = 0$ (also, more points shown). Yellow: Low-pass filtered version of the blue curve. The symmetrisation manoeuvred the time point $t = 0$ to the centre, thus minimising filter end-effects at $t = 0$.

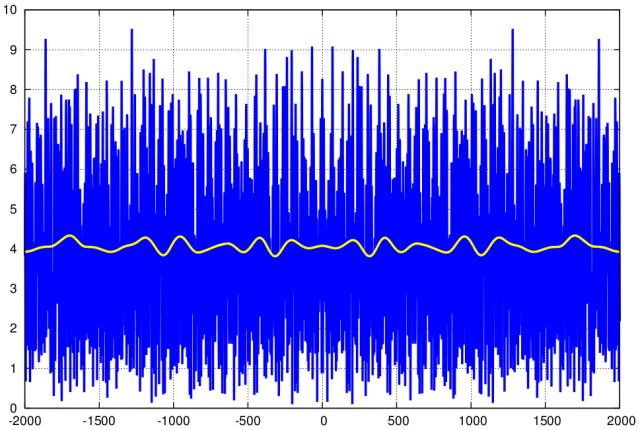

Figure 4. Blue: Absolute value of the complex-valued non-decaying signal $|s(t)^{\text{no\_decay}}|$, in the denominator of the fraction in Eq. (3), and symmetrised as in Fig. 3. Yellow: Low-pass filtered version of the blue curve. The yellow curves of Figs. 3, 4 are blue, red respectively in Fig. 5.

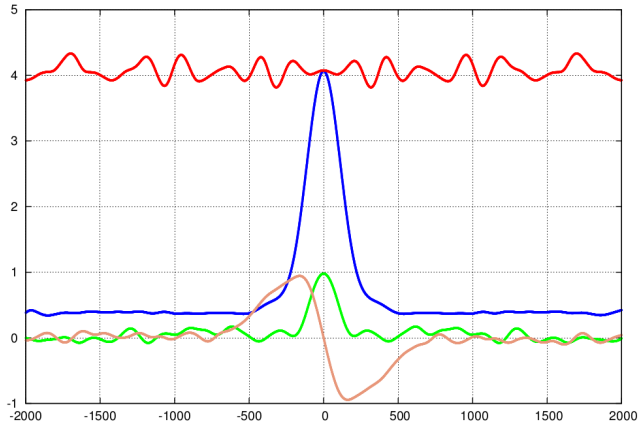

Figure 5. The four separately low-pass filtered components of Eq. (3) which together yield the wanted estimate of the complex-valued temporal decay of the MRS signal, shown in Fig. 6. Green: Re$[e^{\imath\phi(t)}]$. Brown: Im$[e^{\imath\phi(t)}]$. See also the caption of Fig. 4.

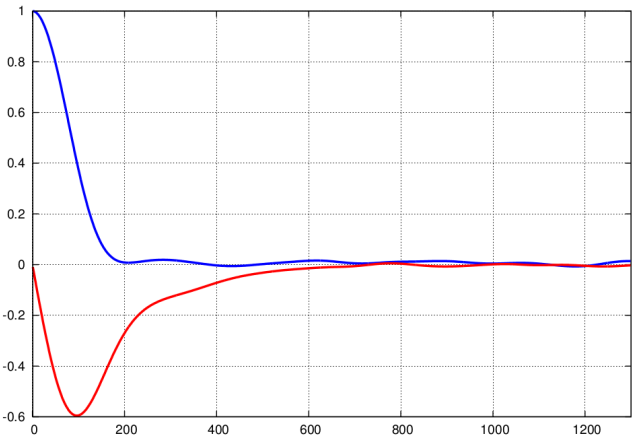

Figure 6. Complex-valued decay $d(t)$, estimated by combining the right-hand halves of the four curves, according to Eq. (3). Blue: Real part. Red: Imaginary part. The over-sensitive division of the blue curves in Figs. 3, 4, applied in the past, has now been replaced by division of the yellow curves. The latter division is robust in the presence of noise in $s(t)$.

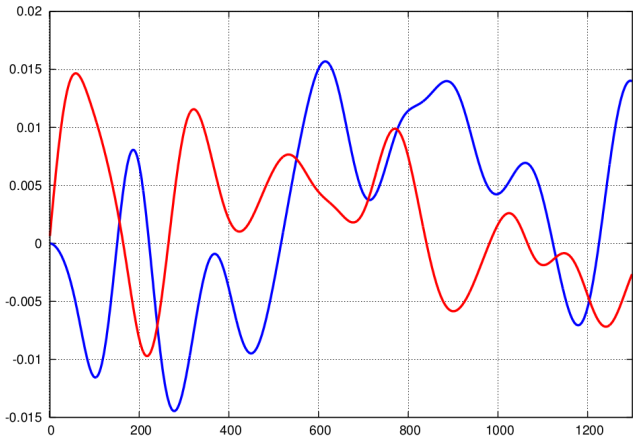

Figure 7. Incurred error: Estimated decay minus true decay. Blue: Real part. Red: Imaginary part. Note that the vertical scale has been expanded considerably. In fact, the error is of the order of one to two percent.

apply the filter to the entire, double-length signal. In this way, the time point $t = 0$ is at maximum distance from either end (edge). In addition, apart from noise, the signal is nearly zero at both ends. As a result, edge-effects of the filter are minimised.

Figs. 2 to 7 provide a graphical display of the procedure just described.

Fig. 2 shows the absolute value of the MRS signal $|s(t)|$ over 1300 sample points. Ten different metabolite species contribute [1]. At sample point 500, the signal has decayed into the noise.

Fig. 3, blue curve, shows the symmetrised version of $|s(t)|$, in the sample point range -2000 to +2000. The yellow curve results from low-pass filtering the blue curve. We point at four aspects: 1) The cut-off frequency of the low-pass filter was set sufficiently low to strongly reduce the oscillations. 2) In the outer wings of the yellow curve, the metabolite signal has decayed to zero. However, the height of these wings is not zero, but is lifted to the average absolute value of the noise. 3) In the central region of the yellow curve, the metabolite signal is *greater* than the noise, making the former act as homodyne detector [4] with long RC-time-constant [5]. As a result, the noise is averaged out in this region. In other words, the noise does not lift the top of the yellow curve. 4) The cut-off frequency of the low-pass filter was nonetheless set sufficiently high to let the yellow curve approach its full value $|s(0)|$; see also Fig. 5, below.

Fig. 4 shows the symmetrised version of $|s(t)^{\text{no\_decay}}|$, which is a synthetic signal composed from a metabolite signal database using approximate metabolite concentrations, initially obtained by using a simple approximate analytical physical decay function, mentioned earlier. The yellow curve is the result of the low-pass filter.

At this stage of the description of the procedure, we can already illustrate graphically the main aspect of our method: Traditionally, one divides the blue curves of Fig. 3, 4; now we divide the yellow curves, taking the phase factor into account, which is very robust.

Fig. 5 shows the four components of Eq. (3) as obtained with the new method. Each is the result of filtering prior to division. At the time origin, $t = 0$, the decay process has yet to begin, so $|s(0)^{\text{no\_decay}}|$ should approximate $|s(0)|$. Indeed, the red and blue low-passed filtered curves (yellow in Fig. 3,4), are seen to coincide at that point of time. Recall from the discussion of Fig. 3, above, that $|s(0)|$ is not lifted upward by the noise. The fact that $d(t)$ approaches zero beyond sample ≈ 600 (next Figure) despite the lifting of the blue curve in that region, is brought about by the low-pass filtered phase factor, represented by the green and brown curves. Details of the shapes of the latter curves are under investigation.

Fig. 6 shows the result of working out Eq. (3); blue: Real part of $d(t)$, red: Imaginary part of $d(t)$. Spikes are absent from sample 0 to sample 1300. The next Figure shows whether this result is acceptable.

[4] http://en.wikipedia.org/wiki/Homodyne_detection
[5] http://en.wikipedia.org/wiki/RC_time_constant

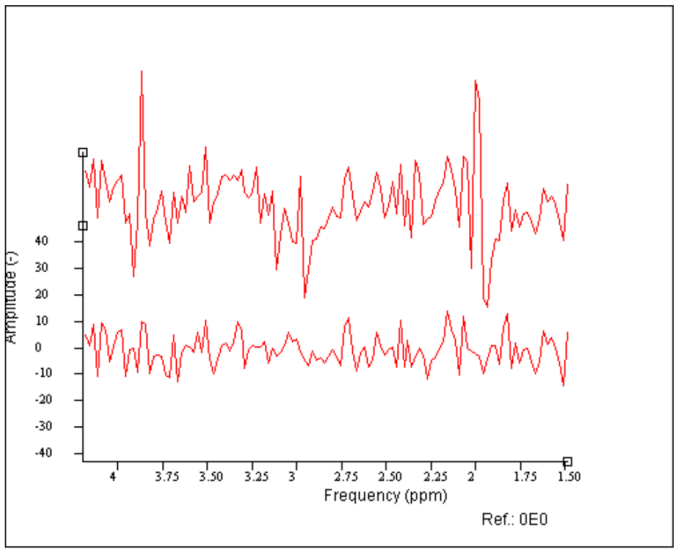

Figure 8. Residues in the spectral domain. Only the first 450 samples were used in the the time-domain fit, resulting is low spectral resolution.
Upper: Mono-exponential decay used, and amplitudes 'normalised'; pertaining to column **B** in Table I. The spectrum is shifted upward from the baseline for better viewing. **Lower:** Decay estimated with present method; pertaining to column **D** in Table I. Graph made with jMRUI [5].

Finally, Fig. 7 shows the difference between the estimated decay and the true decay, with a strongly expanded vertical scale. It turned out that the difference (estimation error) is here only one to two percent; see also point 9 in Sec. IV.
It remains to be seen whether estimation of metabolite concentrations using Eq. (1) and the estimated decay, gives indeed satisfactory results. This will be treated below, in Sec. III.

III. Results

We tested the quality of our estimated decay by means of a Monte Carlo (MC) simulation as described in [1]. The input of the MC simulation comprised the model function of Eq. (1) and a great number, here thousand, of different Gaussian noise realisations with equal standard deviation (stdev) and zero mean that were separately added to the noiseless version of the simulated signal. Each of the resulting thousand different noisy signals was subjected to model fitting with a home-made NLLS program, based on LAPACK, that is easily adaptable to our needs. The output of the MC simulation consists of the mean, bias, and standard deviation of all fitted model parameters. The results for the concentrations are listed in Table I.

IV. Discussion

1) The signal-to-noise ratio (SNR) of our simulated signal is low; see Fig. 2. Nevertheless, Fig. 7 shows that the new method for estimating the decay is not particularly perturbed at this level of the noise.
2) The simulated signal comprises a temporal decay function that deviates significantly from a mono-exponential; see Fig. 1. In fact, we prepare for the imminent introduction [7] of wide-bore magnets for humans operating at a field as high as 11.7 Tesla. At such a high value, tissue microstucture determines the *in vivo* inhomogeneity of the field, and thereby the form of the decay function [8]. Our simulated decay, when transformed to the frequency-domain by FFT, yields a clearly asymmetric shape; see Fig. 1. The *in vivo* decay function for humans at 11.7 Tesla is still unknown.
3) When a model function is partly unknown, estimation of the physical model parameters contained in it, becomes biased [1]. If possible, separate estimation of the unknown part should then be attempted. An estimation without an analytical, physical model, can be referred to as a 'search in *function* space', in contrast to a 'search in physical *parameter* space' when applying NLLS. The resulting numerical function can be used, in fixed form, to complete a model function such as Eq. (1). This was done in the present work.
4) A complication of searching in function space is that new parameters emerge that have to be set at optimal values. Such parameters are called hyper-parameters. In the present case, the hyper-parameter to be set is the cut-off frequency of the low-pass filter. This frequency depends on the signal at hand. A clinician can not be expected to be aware of this. Therefore, hyper-parameters should be optimised automatically during runtime. This can be a very difficult problem. Reliable automatic optimisation of the above-mentioned cut-off frequency is under investigation. So far, it seems to be the only hyper-parameter of the new method, though.
5) As for the main goal of the research, see Table I. The results lie between two extremes, columns **A** and **E**. The numbers in **A** were obtained with a surrogate decay, namely the mono-exponential $d(t) = 1.0 \times \exp(\alpha t)$, where α is included in the NLLS fit. To ensure proper convergence, α was kept equal for each metabolite species during the fit. In column **A**, bias is significantly higher than in other columns, for most metabolite species; therefore, the theory of the Cramér-Rao bound (CRB) does not apply. The numbers in column **E** were obtained with the *true* decay. The model function being complete and correct in that case, the standard deviations approximate the CRB's (not tested so far).
6) The *ratios* of the estimated metabolite concentrations are less sensitive to the inadequacy of assumed mono-exponential decay. This is apparent from the significant improvement obtained from normalisation, *i.e.*, adapting the concentrations such that $s(0)^{\text{no\_decay}} = s(0)$, keeping their ratios constant; see column **B**. Should this result be generally true, then why bother to still estimate $d(t)$? We offer the following consideration: If one reconstructs a signal using good estimated parameters but an incorrect decay function, then the 'residue'[6] will not look good. Understandably, clinicians are suspicious and will reject

[6]In metabolite quantitation with MRS, achieving a noise-like residue in the spectral (frequency) domain is indispensable.

Table I

Result of Monte Carlo simulation using Eq. (1) and thousand different noise realisations.

The signal-to-noise ratio (SNR) can be gleaned from Fig. 2. **m** = number of metabolite species. **mean** = mean metabolite concentration resulting from the Monte Carlo simulation. **error** = bias, standard deviation (stdev), rmse (root mean square error).
A = real-valued mono-exponential $d(t)$. **B** = as **A**, but concentrations are normalised. **C** = as **B**, but all $\triangle\nu_m$ are kept equal during the fit. using estimated $d(t)$. **D** = using *estimated* $d(t)$. **E** = as **D**, but using true $d(t)$.. Negative outcomes, occurring with bias, are printed red.

m	error	A	B	C	D	E
1	mean	2.14364	1.76495	1.76593	1.74909	1.75544
1	bias	0.38866	0.00998	0.01096	-0.00589	0.00047
1	stdev	0.03803	0.06612	0.06606	0.03336	0.03161
1	rmse	0.39052	0.06687	0.06697	0.03387	0.03161
2	mean	0.29387	0.24191	0.22688	0.16618	0.16667
2	bias	0.10178	0.04982	0.03478	-0.02592	-0.02543
2	stdev	0.07966	0.06610	0.06441	0.10653	0.10790
2	rmse	0.12924	0.08277	0.07320	0.10964	0.11086
3	mean	2.45239	2.01916	2.01879	2.06064	2.06727
3	bias	0.38504	-0.04819	-0.04855	-0.00671	-0.00008
3	stdev	0.03842	0.07374	0.07366	0.03300	0.03182
3	rmse	0.38695	0.08809	0.08822	0.03367	0.03182
4	mean	1.64442	1.35395	1.35411	1.35075	1.35559
4	bias	0.28817	-0.00231	-0.00215	-0.00551	-0.00066
4	stdev	0.03815	0.05507	0.05514	0.03189	0.03091
4	rmse	0.29068	0.05512	0.05518	0.03236	0.03092
5	mean	0.67436	0.55522	0.53362	0.64143	0.64054
5	bias	0.04136	-0.07779	-0.09939	0.00842	0.00753
5	stdev	0.06629	0.05745	0.05629	0.05937	0.08535
5	rmse	0.07813	0.09670	0.11422	0.05997	0.08568
6	mean	0.14817	0.12203	0.07778	0.05870	0.03991
6	bias	0.00094	-0.02521	-0.06945	-0.08853	-0.10732
6	stdev	0.13924	0.11471	0.06819	0.14011	0.13466
6	rmse	0.13924	0.11745	0.09733	0.16574	0.17219
7	mean	0.70635	0.58157	0.58248	0.54870	0.55279
7	bias	0.15360	0.02882	0.02973	-0.00405	0.00004
7	stdev	0.02478	0.02786	0.02790	0.02024	0.01985
7	rmse	0.15559	0.04008	0.04077	0.02064	0.01985
8	mean	3.61377	2.97537	2.97626	2.96242	2.97463
8	bias	0.63954	0.00114	0.00203	-0.01181	0.00040
8	stdev	0.04394	0.10439	0.10431	0.04138	0.03686
8	rmse	0.64105	0.10439	0.10433	0.04303	0.03687
9	mean	0.81617	0.67200	0.67124	0.65541	0.65680
9	bias	0.15530	0.01113	0.01037	-0.00546	-0.00407
9	stdev	0.03174	0.03447	0.03460	0.02649	0.02640
9	rmse	0.15851	0.03622	0.03612	0.02704	0.02671
10	mean	0.17600	0.14493	0.14182	0.12168	0.12347
10	bias	0.05609	0.02502	0.02191	0.00176	0.00356
10	stdev	0.03445	0.02886	0.02890	0.03289	0.03465
10	rmse	0.06583	0.03819	0.03627	0.03294	0.03484

a quantitation, when the residue of their NLLS fit does not resemble pure noise.

7) Column **C** is as **B**, but now with the frequency shifts $\triangle\nu_m$ locked together during the fit to improve its convergence. There seems to be no consistent effect of this measure in the Table.
8) The results of metabolite quantitation with *estimated* decay are displayed in column **D**. The most significant effect of estimating $d(t)$ is for species 1, 3, 4, 8 whose concentrations are highest; note that bias $\ll$ standard deviation for these species. For species 2 and 6, little effect of using *estimated* decay is found, but that applies even to using the *true* decay as listed in column **E**. When the order of magnitude of the standard deviation is of the order of magnitude of the concentration, one can not expect more. Metabolite species 10, whose concentration is lowest, while its errors approach those of the concentrated species, is a case apart; see Table II in the Appendix.
9) As mentioned in Sec. II, in the past the effect of noise on the division in Eq. (3) was addressed after the division had been carried out. To this end, low-pass filtering based on splines, wavelets, or exponentially damped sinusoids was used. In the present work, we apply a Butterworth 3 low-pass filter (LP), *before* the division. This amounts to approximating the LP of the full expression in Eq. (3) by the LP of its separate constituents, according to :

$$\mathrm{LP}[d(t)] \approx \frac{\mathrm{LP}[|s(t)|]}{\mathrm{LP}[|s(t)^{\mathrm{no\_decay}}|]}\,\mathrm{LP}[e^{\imath\phi(t)}] \qquad (4)$$

Simulations without noise indicated the order of magnitude of the error incurred in Eq.(4). This aspect is to be investigated further. At *high* SNR, estimation of $d(t)$ by yet another method, involving a genetic algorithm named 'pikaia', is recommended [2,9].
10) The present simulated signal lacks a contribution from so-called macromolecules (MM) [4]. In clinical practice, this simplification is not very realistic. The matter is perhaps handled best by separate measurement of the MM signal with so-called 'inversion recovery' [4], and subsequent subtraction of this MM signal from the full MRS signal, at least while estimating $d(t)$.

V. Concluding Remarks

We devised a simple and robust estimator of the generally unknown temporal decay of *in vivo* metabolite signals obtained from an MRI scanner. The estimated temporal decay serves to complete the metabolite model function for analysing signals measured non-invasively in patients. This obviates the use of an approximative surrogate decay function which can cause biased results. The new estimator not only reduces bias but also improves the spectral residue of model function fitting, thus raising confidence of clinical users.

Acknowledgement

This work was done in the context of FP7 - PEOPLE Marie Curie Initial Training Network Project PITN-GA-2012-316679-TRANSACT, http://www.transact-itn.eu/index.php, based in part on the free software package jMRUI, http://www.mrui.uab.es/mrui/.

References

[1] D. van Ormondt, R. de Beer, D.M. Sima, and D. Graveron-Demilly, "Error-Bars in Semi-Parametric Estimation," in *ProRISC, ICT.OPEN*. Eindhoven, The Netherlands: IPN, STW, NWO, 27-28 November 2013, pp. 15–20, http://www.ictopen2013.nl/content/proceedings+2013. 1, 2, 3, 4, 6

[2] ——, "New Approach to Semi-Parametric Estimation for *In Vivo* Magnetic Resonance Spectroscopy," in *ProRISC, ICT.OPEN*. Veldhoven, The Netherlands: IPN, STW, NWO, 27-28 November 2011, pp. 45–50. 1, 6

[3] M.I. Osorio-Garcia, D.M. Sima, F.U. Nielsen, T. Dresselears, F. Van Leuven, U. Himmelreich, and S. Van Huffel, "Quantification of in vivo ^{1}H Magnetic Resonance Spectroscopy (MRS) signals with baseline and lineshape estimation ," *Meas. Sci. Technol.*, vol. 22, 2011, http://iopscience.iop.org/0957-0233/22/11/114011. 1

[4] D. Graveron-Demilly, "Quantification in Magnetic Resonance Spectroscopy Based on Semi-Parametric Approaches," *Magn Reson Mater Phy*, vol. 27, no. 2, pp. 113–130, April 2014. 1, 6

[5] D. Stefan, F. Di Cesare, A. Andrasescu, E. Popa, A. Lazariev, E. Vescovo, O. Strbak, S. Williams, Z. Starcuk, M. Cabanas, D. van Ormondt, and D. Graveron-Demilly, "Quantitation of magnetic resonance spectroscopy signals: The jMRUI software package," *Meas. Sci. Technol.*, vol. 20, 2009, http://iopscience.iop.org/0957-0233/20/10/104035/. 1, 4

[6] P.B. Pynsent and R. Hanka, "A simple program for a phaseless recursive digital filter," *Journal of Biomedical Engineering*, vol. 4, no. 3, pp. 252–254, July 1982, doi:10.1016/0141-5425(82)90011-5. 2

[7] H. Kanithi, D. Blasiak, J. Lajewski, C. Berriaud, P. Vedrine, and G. Gilgrass, "Production Results of 11.75 Tesla Iseult/INUMAC MRI Conductor at Luvata - art. no. 6000504." *IEEE Transactions on Applied Superconductivity*, vol. 24, no. 3, p. 504, 2014. 4

[8] D.K. Deelchand, P-F. Van de Moortele, G. Adriany, I. Iltis, P. Andersen, J.P. Strupp, J.P. Vaughan, K. Uğurbil, and P-G. Henry, "*In vivo* ^{1}H NMR spectroscopy of the human brain at 9.4 T: Initial results," *Journal of Magnetic Resonance*, vol. 206, pp. 74–80, 2010. 4

[9] D. van Ormondt, R. de Beer, D.M. Sima, and D. Graveron-Demilly, "Bias-Variance Trade-Off in In Vivo Metabolite Quantitation," in *ProRISC, ICT.OPEN*. Rotterdam, The Netherlands: IPN, STW, NWO, 22-23 October 2012, p. 10 pp. 6

Appendix I

Table II
Names and concentrations (amplitudes) of metabolites involved in this work [1]

m	Abbreviated	Metabolite name	True amplitudes
1	Cho1	choline singlet	1.75497
2	Cho2	choline multiplet	0.19210
3	Cr1	creatine singlet 1	2.06735
4	Cr2	creatine singlet 2	1.35626
5	Glu	glutamate	0.63300
6	Gln	glutamine	0.14723
7	mI	myo-inositol	0.55275
8	NAA1	NAA singlet	2.97423
9	NAA2	NAA multiplet	0.66087
10	sI	scyllo-inositol	0.11991